HIGH THROUGHPUT SPECTRAL IMAGING SYSTEM FOR WHOLESOMENESS INSPECTION OF CHICKEN

K. Chao, C.-C. Yang, M. S. Kim, D. E. Chan

ABSTRACT. *An online line-scan imaging system containing an electron-multiplying charge-coupled device detector and line-scan spectrograph was used for identifying wholesome and unwholesome freshly slaughtered chicken carcasses on high-speed commercial chicken processing lines. Hyperspectral images were acquired using the line-scan imaging system for 5549 wholesome chicken carcasses and 93 unwholesome chicken carcasses on a commercial processing line, for analysis to optimize ROI size and location and to determine the key intensity waveband and ratio wavebands to be used for online inspection. Multispectral imaging algorithms were developed for real-time online identification of wholesome and unwholesome chicken carcasses. The imaging system inspected over 100,000 chickens on a commercial 140-bpm kill line during continuous operation and achieved over 99% accuracy in identifying wholesome chickens and over 96% accuracy in identifying unwholesome chickens. A system of this type can perform food safety inspection tasks accurately and with less variation in performance at high speeds (e.g., at least 140 bpm), and help poultry plants to improve production efficiency and satisfy increasing consumer demand for poultry products.*

Keywords. *Food safety, HACCP, Poultry, Spectral imaging.*

The 1957 Poultry Product Inspection Act mandated postmortem inspection of every bird carcass processed by a commercial facility. Since then, USDA inspectors have conducted on-site organoleptic inspection of all chickens processed at U.S. poultry plants for indications of diseases or defects. Inspectors of the USDA Food Safety and Inspection Service (FSIS) examine by sight and by touch the body, the inner body cavity surfaces, and the internal organs of every chicken carcass during processing operations.

With the 1996 final rule on Pathogen Reduction and Hazard Analysis and Critical Control Point (HACCP) systems (USDA, 1996), FSIS implemented the HACCP and Pathogen Reduction programs in meat and poultry processing plants throughout the country to prevent food safety hazards. More recently, FSIS has also been testing the HACCP-Based Inspection Models Project (HIMP) in a small number of volunteer plants (USDA, 1997). HIMP requirements include zero tolerance for unwholesome chickens exhibiting symptoms of "septox" – a condition of either septicemia or toxemia. Wholesome chickens do not exhibit symptoms of "septox" and the unwholesome birds must be removed from the processing line.

Septicemia is caused by the presence of pathogenic microorganisms or their toxins in the bloodstream, and toxemia results from toxins produced by cells at a localized infection or from the growth of microorganisms. Septox birds are considered to be unwholesome and USDA inspectors remove these unwholesome birds from the processing lines during their bird-by-bird inspections, which can, by law, be conducted at a maximum speed of 35 birds per minute (bpm) for an individual inspector. The inspection process is subject to human variability, and the inspection speed restricts the maximum possible output for the processing plants while also making inspectors prone to fatigue and repetitive injury problems. This limit on production throughput, combined with increases in chicken consumption and demand over the past two decades, places additional pressure on both chicken production and the food safety inspection system. U.S. poultry plants now process over 8.8 billion broilers annually (USDA, 2007). During processing at a typical U.S. poultry plant, birds are first slaughtered on kill lines and then transferred to evisceration lines on which inspection stations are located. Commercial evisceration lines in the United States currently may be operated at speeds up to 140 bpm; however, such processing lines require up to four inspection stations, each with an FSIS inspector to conduct bird-by-bird inspection at the 35-bpm speed limit.

Machine vision technologies have been developed to address a variety of food and agricultural processing applications. Various sensing techniques such as RGB (red/green/blue) color imaging, visible and near-infrared (Vis/NIR) spectroscopy and imaging, fluorescence spectroscopy and imaging, and X-ray imaging, have been investigated for potential use in food processing and online inspection applications (Daley et al., 1994; Delwiche, 2003; Jing et al., 2003; Kim et al., 2003; Lu, 2007; Windham et al., 2003).

Submitted for review in November 2007 as manuscript number FPE 7282; approved for publication by the Food & Process Engineering Institute of ASABE in April 2008.

Mention of a product or specific equipment does not constitute a guarantee or warranty by the U.S. Department of Agriculture and does not imply its approval to the exclusion of other products that may also be suitable.

The authors are **Kuanglin Chao,** Research Scientist, USDA-ARS Food Safety Laboratory, Beltsville, Maryland; **Chun-Chieh Yang, ASAE Member,** Research Associate, Department of Biosystems and Agricultural Engineering, University of Kentucky, Lexington; **Moon S. Kim,** Research Physical Scientist, and **Diane E. Chan,** Agricultural Engineer, USDA-ARS Food Safety Laboratory, Beltsville, Maryland. **Corresponding author:** Kuanglin Chao, Food Safety Laboratory, USDA-ARS, Building 303, BARC-East, 10300 Baltimore Ave., Beltsville, MD 20705; phone: 301-504-8450; fax: 301-504-9466; e-mail: kevin.chao@ars.usda.gov.

A variety of methods for imaging whole chicken carcasses and chicken viscera/organs have been investigated for use in food safety inspection of poultry. RGB color imaging of chicken spleens, hearts, and livers was found capable of identifying poultry disease conditions including leucosis, septicemia, airsacculitis, and ascites in the laboratory (Tao et al., 1998; Chao et al., 1999), but these methods required precise presentation of the visceral organs and thus were unsuitable for conventional poultry processing lines. A two-camera system using two wavebands in the visible spectrum for whole-carcass imaging was able to separate 90% of wholesome and unwholesome chickens at processing line speeds up to 70 bpm, but was not feasible for higher speed processing (Park and Chen, 2000; Chao et al., 2002).

Thus there remains a need to develop imaging systems that can inspect chickens for wholesomeness in commercial processing lines which operate at speeds of at least 140 bpm. The objectives of this study were to provide an online line-scan imaging system capable of both hyperspectral and multispectral visible/near-infrared reflectance, and a method of using the system to inspect freshly slaughtered chickens on a processing line for wholesomeness and unwholesomeness.

Materials and Methods

High Throughput Spectral Imaging System

The spectral imaging system (fig. 1) consisted of an Electron-Multiplying Charge-Coupled-Device (EMCCD) camera, an imaging spectrograph, a C-mount lens, and a pair of high power, broad-spectrum white light-emitting-diode (LED) line lights. The EMCCD camera (PhotonMAX 512b, Roper Scientific, Inc., Trenton, N.J.) has approximately 512 × 512 pixels and is thermoelectrically cooled to approximately -70°C (via a three-stage Peltier device). An imaging spectrograph (ImSpector V10 OEM, Specim/Spectral Imaging Ltd., Oulu, Finland), and a C-mount lens (Rainbow S6x11, International Space Optics, S.A., Irvine, Calif.) are attached to the EMCCD imaging device. The spectrograph aperture slit of approximately 50 microns limits the instantaneous field of view (IFOV) of the imaging system to a thin line. Light from the linear IFOV is dispersed by a prism-grating-prism line-scan spectrograph and projected onto the EMCCD imaging device. The spectrograph creates a two-dimensional (spatial and spectral) image for each line-scan, with the spatial dimension along the horizontal axis and the spectral dimension along the vertical axis of the EMCCD imaging device. The imaging device is coupled with a 16-bit digitizer (CCI-23, Andor Technology Limited, South Windsor, Conn.) with a pixel-readout rate of approximately 10 MHz. The digitizer performs rapid analog-to-digital conversion of the image data for each hyperspectral or multispectral line-scan image. These data are then processed by the computer for image analysis and classification of wholesome and unwholesome pixels in the line-scan images.

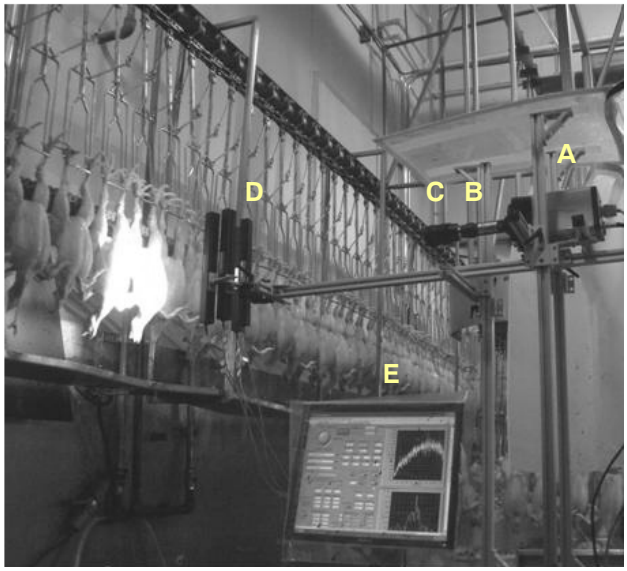

Figure 1. A photograph of the hyperspectral/multispectral imaging inspection system on a commercial chicken processing line. A: Electron-Multiplying Charge-Coupled-Device (EMCCD) camera; B: line-scan spectrograph; C: lens assembly; D: LED lighting system; E: data processing unit.

The spectral imaging system requires calibration before line-scan images can be acquired. Re-calibration is generally not required unless the physical arrangement of the components of the imaging system is disturbed. The first step in the calibration process was to cool the imaging system to its operating temperature of -70°C. The next step was to set image binning, which is determined by the spectral distribution of useful wavelengths and the size of spatial image features to be processed for the application. The original image size, 512 × 512 pixels, was reduced by 1 × 4 binning to result in line-scan images with a spatial resolution of 512 pixels (512 divided by 1) and a spectral resolution of 128 pixels (512 divided by 4) in the spectral dimension. The binning process adds together photons from adjacent pixels in the detector array and was performed by the shift register of the EMCCD imaging device. This produced a reduced number of pixels to be digitized by the 16-bit A/D PCI board for the computer to process. Reducing total pixel readout time decreased the acquisition time of each line-scan image, which allowed higher image acquisition speed for the EMCCD imaging device. Because the useful spectrum of light did not span the entire width of the EMCCD detector, the first 20 and last 53 spectral bands were discarded, resulting in a line-scan image size of 512 × 55 pixels.

The next step in the calibration process was spectral waveband calibration that identified each spectral channel with a specific wavelength. A neon-mercury calibration lamp (Oriel Instruments, Stratford, Conn.) was utilized for spectral calibration; the mercury peaks at 435.84 and 546.07 nm were found to correspond to the 8th and 25th bands, respectively, and neon peaks at 614.31, 640.23, 703.24, and 724.52 nm corresponded to the 35th, 39th, 49th, and 52nd bands, respectively. The following second-order polynomial regression was calculated from the reference wavelength peaks of the mercury and neon spectra to calibrate the spectral axis:

$$\lambda = 0.01 \times n_c^{\,2} + 6.03 \times n_c + 393.70 \quad (r^2 = 0.9999) \qquad (1)$$

where λ is the wavelength (nm), and n_c is the spectral channel number. The hyperspectral imaging data ranged from 399.94 nm (the first band) to 750.42 nm (the 55th band) with an average bandwidth of 6.02 nm. The distance between the lens and IFOV target area was 914 mm, with the LED line lights illuminating the IFOV target area from a distance of

214 mm. The IFOV spanned 177.8 mm, which translated into 512 spatial pixels, with each pixel representing an area of 0.12 mm^2.

Following system calibration, the spectral imaging system was ready to use for the acquisition of reference line-scan images. Prior to acquiring hyperspectral chicken images, acquisition of a white reference image was performed using a 99% diffuse reflectance standard (Spectralon, LabSphere, Inc., North Sutton, N.H.) illuminated by the lighting system; acquisition of a dark reference image was performed by acquiring an image with the lens covered by a non-reflective opaque black fabric. These reference line-scan images were used to calculate the pixel-based relative reflectance for raw line-scan images as follows:

$$I = \frac{I_0 - D}{R - D} \quad (2)$$

where I is the relative reflectance, I_0 is the raw reflectance, D is the dark reference, and R is the white reference.

Procedures

Following spectral and spatial calibration of the imaging system, hyperspectral line-scan images were acquired for 5549 wholesome chicken carcasses and 93 unwholesome chicken carcasses on a 140-bpm commercial processing line in March 2007. The wholesome or unwholesome condition of the birds on the line was identified by an FSIS veterinarian who observed the birds before they passed through the illuminated IFOV, where the imaging system acquired 55-band hyperspectral data for the chicken carcasses. These hyperspectral images were analyzed for Region of Interest (ROI) optimization and selection of one key wavelength and two ratio wavebands based on average spectral differences between wholesome and unwholesome birds.

Using only the key wavelength and ratio wavebands that were selected by the hyperspectral analysis described above, random track mode on the same imaging system was implemented for multispectral inspection. LabView software (National Instruments Corp., Austin, Tex.) was used to develop software modules for detecting the starting point (SP) and ending point (EP) of each bird, and for implementing classification algorithms based on fuzzy logic. During two 8-h shifts in July 2007, the imaging system conducted multispectral inspection for over 100,000 birds at a commercial processing line. A FSIS veterinary medical officer identified bird conditions during several 30- to 40-min periods for verification of system performance.

Hyperspectral Image Analysis

Analysis of the hyperspectral relative reflectance images began with removal of the background. A relative reflectance threshold value of 0.1 was set for the 620-nm waveband. For any spatial pixel in the hyperspectral reflectance image, the pixel was identified as a background pixel if its reflectance at 620 nm was lower than the 0.1 threshold value. The value of the relative reflectance for every pixel identified as a background pixel was re-assigned to be zero, thus removing these pixels from further image analysis.

The background-removed relative reflectance line-scan images were compiled to form hyperspectral image cubes of entire wholesome and unwholesome chicken carcasses. Using MATLAB software (MathWorks, Natick, Mass.), the hyperspectral chicken images were then analyzed to optimize the spatial ROI within the chicken images. The optimized ROI was one which provided the greatest spectral difference between averaged wholesome pixels and averaged unwholesome pixels across all 55 wavebands, which was obtained as follows. Within a bird image, the potential ROI area spanned from an upper border across the breast of the bird to a lower border at the lowest non-background spatial pixel in each line scan, or to the last (512^{th}) spatial pixel if there were no background pixels present at the lower edge of the image. The average relative reflectance spectrum was calculated across all ROI pixels for all wholesome chicken images, and the average relative reflectance spectrum was calculated across all ROI pixels for all unwholesome chicken images. The difference spectrum between the wholesome and unwholesome average spectra was calculated. This calculation was performed for potential ROIs of varying size, as defined by the number of ROI pixels and their vertical coordinate locations within each line-scan, to optimize the ROI size and location by selecting the ROI that produced the greatest maximum value in its difference spectrum. Using the optimized ROI, the waveband corresponding to the greatest spectral difference between averaged wholesome chicken pixels and averaged unwholesome chicken pixels was identified as a key waveband for differentiation of wholesome and unwholesome chicken carcasses by relative reflectance intensity. Again using the optimized ROI, the average wholesome and average unwholesome spectra were analyzed and potential two-waveband ratios were identified as several ratios using wavebands at which the average wholesome and average unwholesome chicken pixel spectra showed local maxima and local minima. The value of each potential band ratio was calculated for the average wholesome chicken pixels and for the average unwholesome chicken pixels. The two-waveband ratio showing the greatest difference in ratio value between average wholesome and average unwholesome chicken pixels was identified for use in differentiating wholesome and unwholesome chicken carcasses. Multispectral imaging inspection used the key wavelength and the two-waveband ratio to differentiate between wholesome and unwholesome chicken carcasses.

Multispectral Inspection of Chicken Carcass

Effective multispectral imaging inspection of wholesome and unwholesome chicken carcasses on a processing line required the capacity for detecting individual bird carcasses, classifying the condition of the chicken carcass, and generating a corresponding output useful for process control, at speeds compatible with online processing line operations. LabVIEW 8.0 (National Instruments Corp., Austin, Tex.) was used to control the spectral imaging system to perform the tasks required for multispectral inspection of chicken carcasses on a poultry processing line. The line-by-line mode of operation was the basis of the following algorithm that was developed to detect the entry of a bird carcass into the IFOV.

Figure 2 shows the line-by-line algorithm for multispectral inspection to detect and classify wholesome and unwholesome chicken carcasses on a processing line. First, a line-scan image was acquired that contains only raw reflectance values at the two key wavebands needed for intensity and ratio differentiation, the raw reflectance data was converted into relative reflectance data, and background

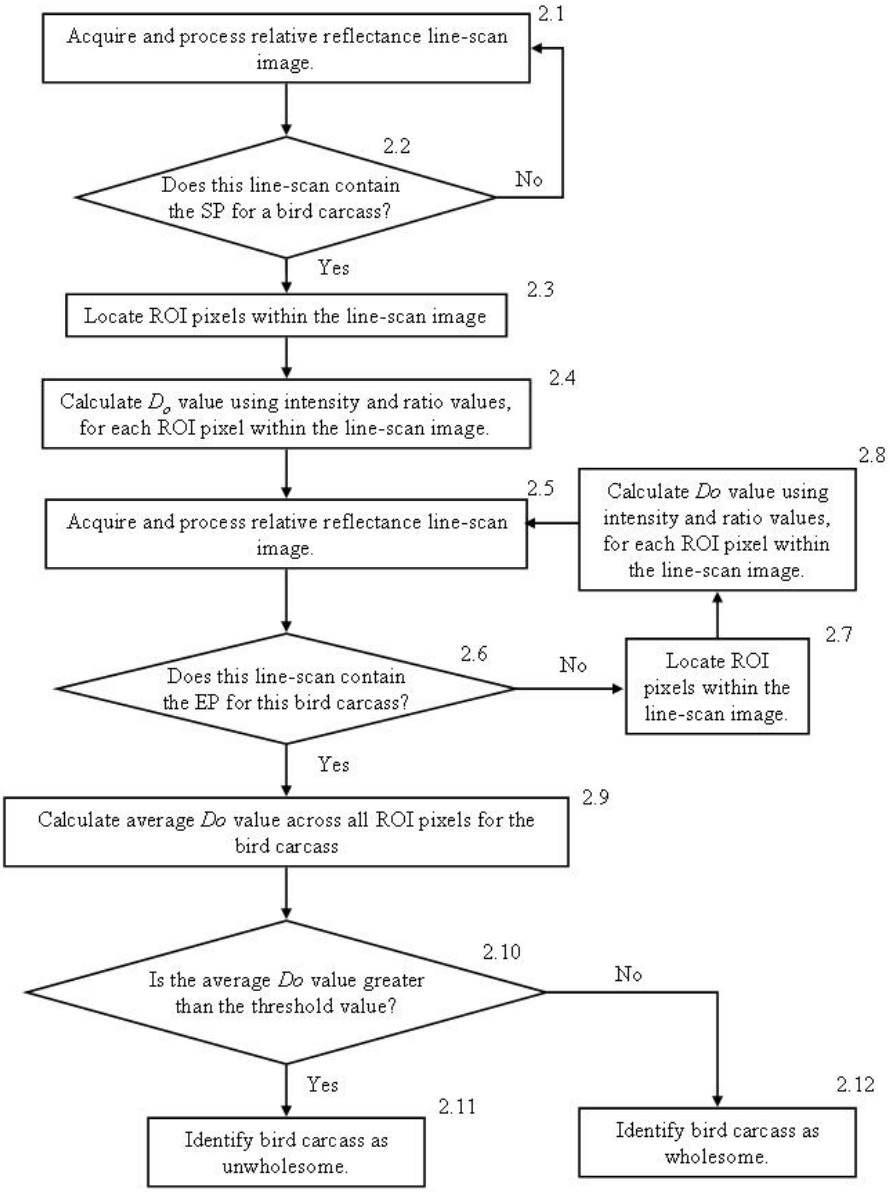

Figure 2. A flowchart of the method for online multispectral line-scan imaging inspection of chickens for wholesomeness.

pixels were removed from the image (fig. 2, Box 2.1). The line-scan image was checked for the presence of the Starting Point (SP) of a new bird (fig. 2, Box 2.2); if no SP was present, no further analysis was performed for this line-scan image and a new line-scan image was acquired. If the line-scan was found to contain an SP, then the ROI pixels were located (fig. 2, Box 2.3) and the decision output value, D_o, was calculated for each pixel in the ROI of the line-scan image fig. 2, Box 2.4). With each new line-scan image acquired (fig. 2, Box 2.5), the ROI pixels were located, and the decision output value of D_o was calculated for each pixel, until the Ending Point (EP) was detected (fig. 2, Box 2.6), indicating no additional line-scan images to be analyzed for the bird carcass. The average D_o value for the bird was calculated (fig. 2, Box 2.9) and compared to the threshold value (fig. 2, Box 2.10) for the final determination of wholesomeness or unwholesomeness for the bird carcass (fig. 2, Boxes 2.11 and 2.12).

With the acquisition of each new line-scan image at the start of the detection algorithm, (fig. 2, Box 2.1), the relative reflectance at 620 nm was examined for each of the first (uppermost) 256 pixels of the line-scan image. The value of the relative reflectance at 620 nm was always at a low-intensity (below 0.1) for these pixels when there was no chicken carcass present in the IFOV. When the relative reflectance at 620 nm increased above 0.1 for any single pixel among the uppermost 256 pixels in the line-scan image, this indicated that a chicken carcass had entered the IFOV. This indication assumed that the inverted chicken carcass was correctly hung from the processing line shackle by both legs and that the entry of the first leg into the IFOV was triggering the detection. The detection algorithm examined only the uppermost 256 pixels in order to disregard carcass wings which were always overlapped between adjacent carcasses on the processing line. After detecting a line-scan image with a single pixel among the uppermost 256 exhibiting relative

reflectance greater than 0.1 at 620 nm, the subsequent line-scan images were monitored as additional pixels within the 256 pixels began showing relative reflectance values greater than 0.1 (fig. 2, Box 2.2). Between the first detected pixel and the 256th pixel, pixels below the first detected pixel began increasing in relative reflectance as the chicken continues to move across the field of view. There would eventually be a line-scan image with one (or several) remaining low-intensity pixel located below the first detected pixel, and above or at the 256th pixel, which was immediately followed by another line-scan in which the previous line-scan's last low-intensity pixel(s) had increased above 0.1. The last low-intensity pixel, or the pixel in the center of the last contiguous group of remaining low-intensity pixels, was identified as the Starting Point (SP) of the bird carcass and represented the junction between the thigh and the abdomen on the leading edge of the carcass.

Similar to the above algorithm, the following algorithm was developed to detect the last relevant line-scan image for each bird as it passed through the IFOV (fig. 2, Box 2.6). After the SP was detected, each subsequent line-scan image was analyzed to determine if the relative reflectance intensity at 620 nm for the pixel matching the vertical coordinate of the SP was above or below 0.1. When a line-scan image was acquired for which that pixel had a relative reflectance intensity at 620 nm that was below 0.1, this pixel was identified as the Ending Point (EP) of the bird carcass, indicating that the main body of the bird had already passed through the IFOV and no further line-scans should be analyzed for that specific bird carcass.

After the initial identification of the SP for a bird carcass, the line-scan image containing the SP and subsequent line-scan images up to the one containing the EP were analyzed, line-by-line (fig. 2, Boxes 2.3 through 2.8), using the following algorithm to classify the bird carcass. For each line-scan image, fuzzy logic membership functions were used to produce two decision outputs for each non-background pixel in the line-scan image that was located within the ROI, using the ROI and waveband parameters previously determined through hyperspectral imaging analysis. For each pixel, two fuzzy logic membership functions were used to generate wholesome and unwholesome fuzzy membership values w_1 and u_1, corresponding to wholesome and unwholesome chickens, from the key wavelength reflectance intensity value for that pixel. Two additional fuzzy logic membership functions were used to generate wholesome and unwholesome fuzzy membership values w_2 and u_2, corresponding to wholesome and unwholesome chickens, from the ratio value for that pixel. The fuzzy inference engine executed a min-max operation (Chao et al., 1999) to obtain a decision output D_o for each pixel based on the n membership functions as follows, where n is the number of criteria input used (in this case, n = 2):

$$D_o = max\,[min\,\{w_1 \ \ldots\ w_n\},\ min\,\{u_1 \ \ldots\ u_n\}]$$

For each pixel, the value of D_o was in the range between 0 and 1, where 0 indicates 100% possibility of wholesomeness and 1 indicated 100% possibility of unwholesomeness. When the EP for that bird carcass was encountered, the average D_o value for all ROI pixels for that bird was calculated (fig. 2, Box 2.9). The bird carcass was identified as being unwholesome if the average D_o value was greater than 0.6; otherwise the chicken carcass was identified as being wholesome (fig. 2, Boxes 2.10, 2.11, 2.12).

Results and Discussion

Analysis of In-Plant Hyperspectral Images

The hyperspectral images were analyzed to optimize the ROI size and location and the key wavebands for differentiation by reflectance intensity and by waveband ratio. Figure 3 shows a contour image of two examples of chicken carcasses with the SP and EP marked and connected by a line on each. The possible size and location of the ROI is described by parameters *m* and *n*, which extended below the

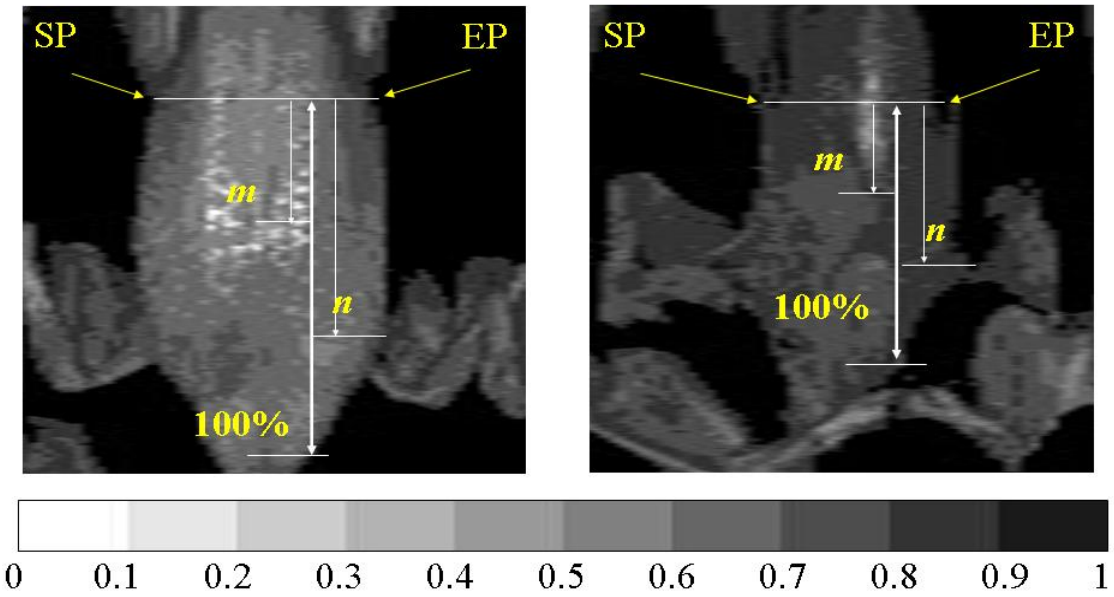

Figure 3. Contour images of two chicken carcasses marked with example locations of the SP, EP, *m*, and *n* parameters used for locating the region of interest.

SP-EP line. The values of *m* and *n* indicated, by percentage of the pixel length between the SP-EP line and the furthest non-background pixel below the SP-EP line, the location of the upper and lower ROI borders. The possible locations of the upper ROI border ranged between a 10% and 40% distance below the SP-EP line, and the possible locations of the lower ROI border range between a 60% and 90% distance below the SP-EP line.

For each possible ROI, the average spectrum across all ROI pixels from the 5549 wholesome chicken carcasses, and the average spectrum across all ROI pixels from the 93 unwholesome chicken carcasses, were calculated. The difference between the average wholesome and average unwholesome value at each of the 55 bands was calculated and their range for each possible ROI is shown in figure 4. Because the 40% to 60% ROI showed the range with the greatest difference values between the average wholesome and unwholesome spectra, this ROI was considered the optimized ROI to be used for multispectral inspection. As shown in figure 5, the 30th band showed the greatest

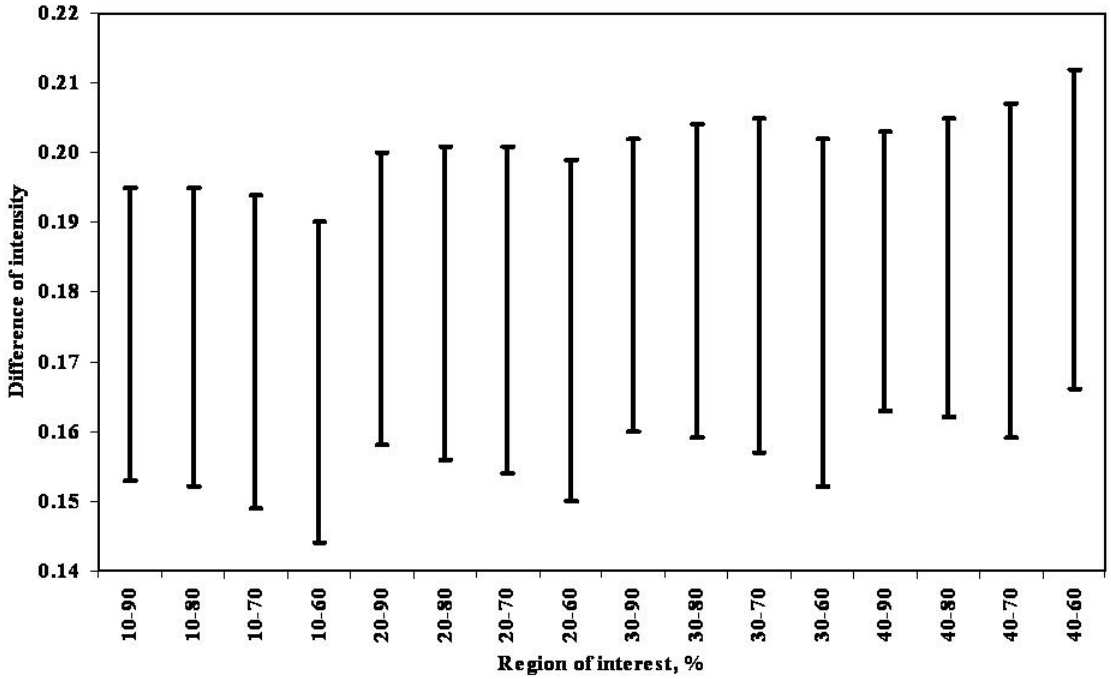

Figure 4. The range, for possible ROIs, of difference values between average wholesome and average unwholesome chicken spectra, for optimizing the ROI to be used for inspection of chickens.

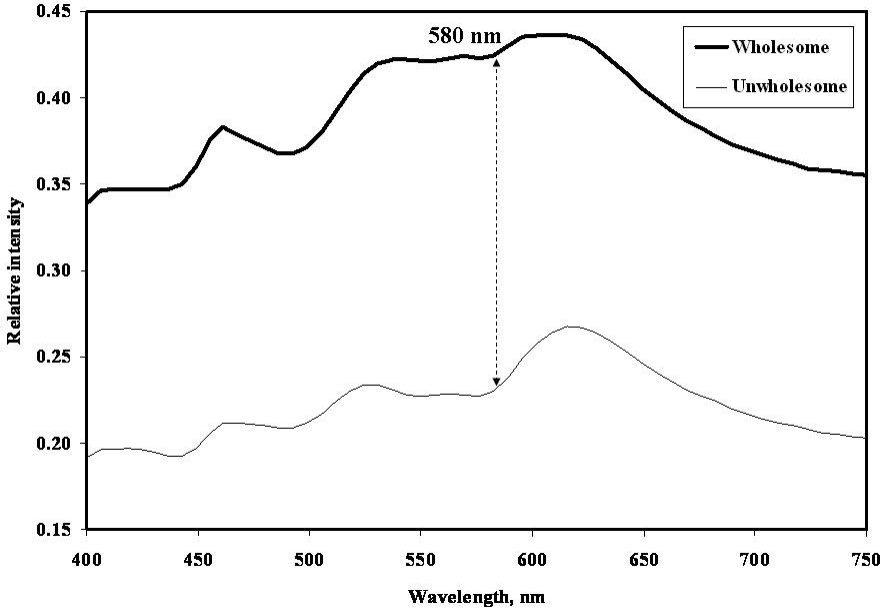

Figure 5. The averaged wholesome and average unwholesome chicken spectra, highlighting the 580 nm key waveband that can be used for intensity-based differentiation of wholesome and unwholesome chickens.

difference between the average wholesome and the average unwholesome spectra from among all 55 bands for the optimized ROI; this band, corresponding to 580 nm, was selected as the key waveband to be used for intensity-based differentiation of wholesome and unwholesome chicken carcasses.

Figure 6 shows the average wholesome and average unwholesome chicken spectra, marked with the wavebands that were investigated for differentiation of wholesome and unwholesome chicken carcasses by a two-waveband ratio. The average wholesome and average unwholesome ratio values were calculated for three possible two-waveband ratios, using wavebands at 440 and 460 nm, 500 and 540 nm, and 580 and 620 nm. The following differences were then calculated:

$$W_{440}/W_{460} - U_{440}/U_{460} = 0.003461$$
$$W_{500}/W_{540} - U_{500}/U_{540} = 0.038602$$
$$W_{580}/W_{620} - U_{580}/U_{620} = 0.115535$$

The last ratio, using the 580- and 620-nm wavebands, showed the greatest difference between the average wholesome and average unwholesome chicken spectra and was thus selected for use in differentiation by two-waveband ratio.

The optimized ROI and key wavebands determined from the hyperspectral data analysis were used for multispectral inspection of over 100,000 chickens on a 140-bpm processing line during two 8-h shifts at a commercial poultry plant. Figure 7 shows examples of chicken images highlighting the ROI that was used for online inspection. The inspection program specifically determined the 40% to 60% ROI for each bird, which was clearly affected by the size and position of the bird. The ROI was a regular rectangular area for a bird whose body extended past the lower edge of the image, such as the first bird in figure 7. For other birds, the presence of background pixels near the lower edge of the image resulted in irregularly shaped ROIs.

Table 1 shows the mean and standard deviation values for relative reflectance at 580 nm for wholesome and unwholesome birds in three data subsets drawn from the hyperspectral data analysis using the 40% to 60% ROI and each of the two

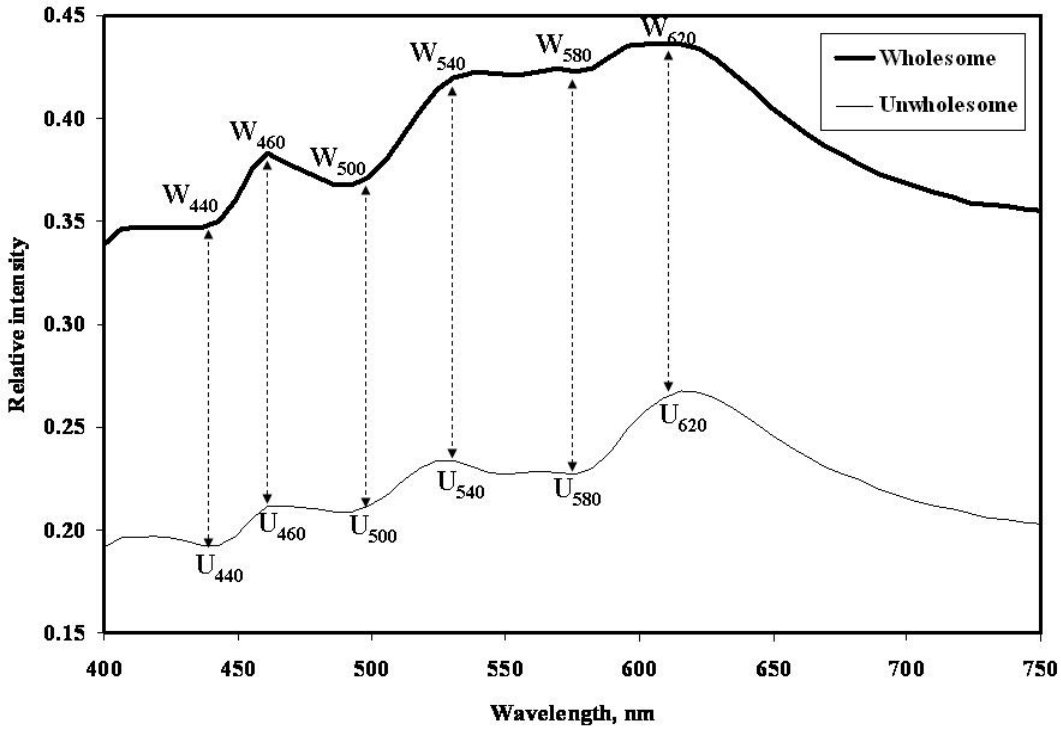

Figure 6. The averaged wholesome and average unwholesome chicken spectra, for possible key wavebands that can be used for two-waveband ratio differentiation of wholesome and unwholesome chickens.

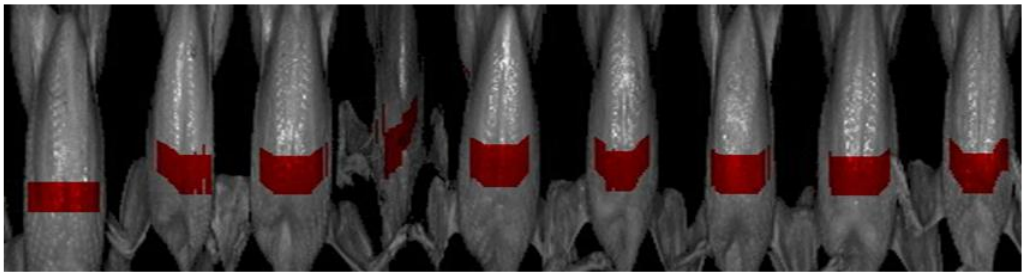

Figure 7. Nine chicken images with the optimized ROI highlighted on each chicken.

Table 1. Mean and standard deviation (SD) values for reflectance intensity at 580 nm for wholesome and unwholesome chicken images.

	Wholesome		Unwholesome	
	Mean	SD	Mean	SD
Hyperspectral analysis	0.378	0.088	0.243	0.076
Inspection shift 1	0.419	0.115	0.253	0.069
Inspection shift 2	0.398	0.083	0.253	0.075

Table 2. Mean and standard deviation (SD) values for two-waveband ratio using 580 and 620 nm for wholesome and unwholesome chicken images.

	Wholesome		Unwholesome	
	Mean	SD	Mean	SD
Hyperspectral analysis	0.948	0.037	0.904	0.052
Inspection shift 1	0.958	0.033	0.918	0.048
Inspection shift 2	0.941	0.038	0.919	0.048

inspection shifts. Table 2 shows the mean and standard deviation values for the two-waveband ratio using 580 and 620 nm for wholesome and unwholesome birds for the same three data subsets. Paired t-tests showed no significant differences (P = 0.05) between the three data sets for the wholesome means, and similarly no significant difference between the three data sets for the unwholesome means. This demonstrates that when the spectral imaging system is appropriately and consistently operated to maintain proper distance and illumination conditions, hyperspectral data collected by the system can be appropriately used for multispectral inspection conducted at different times and locations.

In-Plant Testing of Multispectral Inspection

For multispectral classification, fuzzy logic membership functions were built based on the mean and standard deviation values for the 580-nm key waveband from the hyperspectral analysis data subset, and on the mean and standard deviation values for the 580- and 620-nm two-waveband ratio, again from the hyperspectral analysis data subset. Figure 8 shows the structure of the fuzzy logic membership functions. These functions were used to classify each ROI pixel within an image as either wholesome or unwholesome, by using each pixel's 580-nm intensity value and its ratio value using 580 and 620 nm as inputs to obtain a decision output value D_o between 0 and 1. The average D_o value for a bird was used to determine a wholesome or unwholesome assignment by comparison with a threshold value. Figure 9 first shows a masked image of nine chickens with all ROI pixels highlighted for each chicken (top), and then another image highlighting only those ROI pixels that were classified as wholesome pixels (bottom), i.e., D_o values of individual pixels were each compared to the 0.6 threshold value. The fourth chicken from the left is an unwholesome bird and all of its ROI pixels were identified as unwholesome, consequently not appearing in the second image (bottom).

Figures 10 and 11 show scatterplots of the imaging system's decision outputs against the number of ROI pixels for each chicken imaged during inspection shifts 1 and 2. The total numbers of wholesome and unwholesome chickens identified by the system are shown in table 3, compared with numbers drawn from FSIS tally sheets created by three inspection stations on the same processing line during those two inspection shifts. Although direct bird-to-bird comparison between the imaging inspection system and the inspectors was not performed, the percentages indicated that the relative numbers of wholesome and unwholesome identified by the imaging inspection system and by the processing line inspectors were similar.

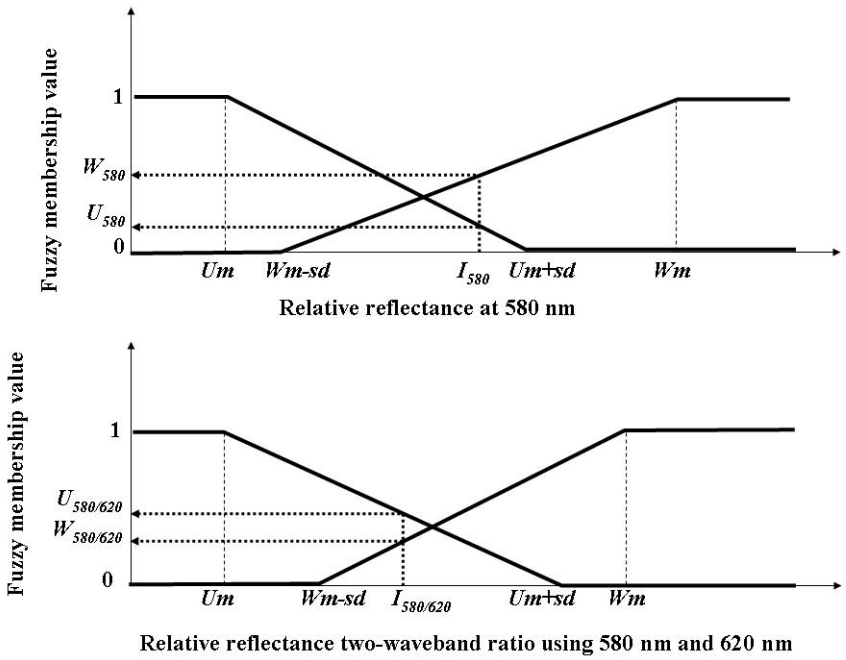

Figure 8. The structure of the fuzzy logic membership functions which use the intensity-based input value (I_{580}) and ratio-based input value ($I_{580/620}$) to create pixel-based decision outputs for wholesomeness classification. W_m: wholesome mean; U_m: unwholesome mean; $W_{m\text{-}sd}$: wholesome mean minus one standard deviation; U_{m+sd}: wholesome mean plus one standard deviation.

Figure 9. A masked image (top) of nine chickens that highlights the ROI pixels to be analyzed for each chicken, and a second image (bottom) highlighting the ROI pixels for each chicken that were classified as wholesome.

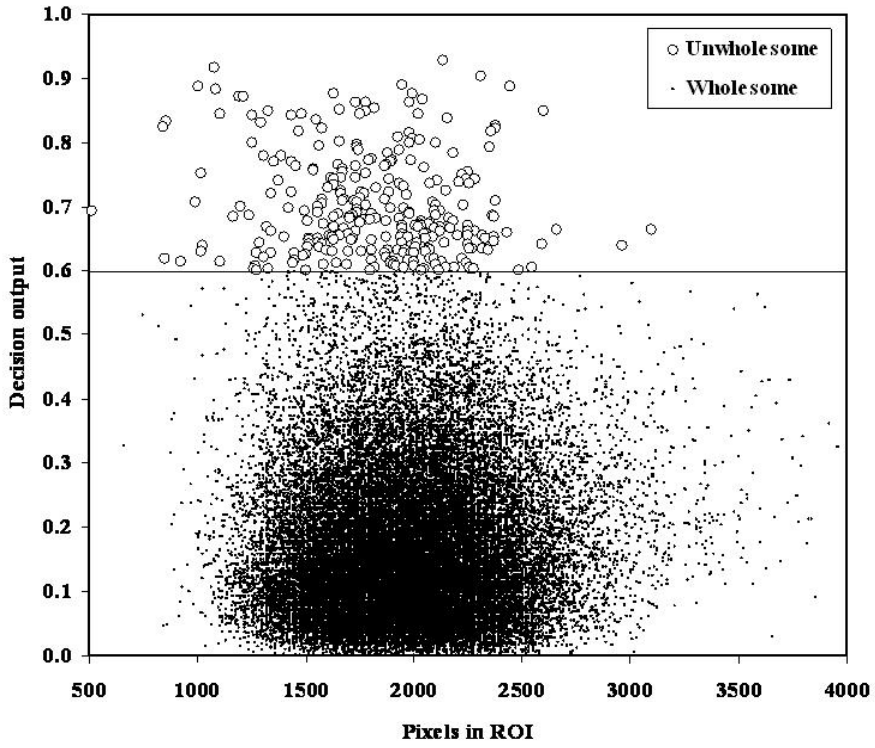

Figure 10. A scatterplot graph showing the distribution of chicken carcasses imaged during inspection shift 1, by the number of ROI pixels and the final decision output for each chicken.

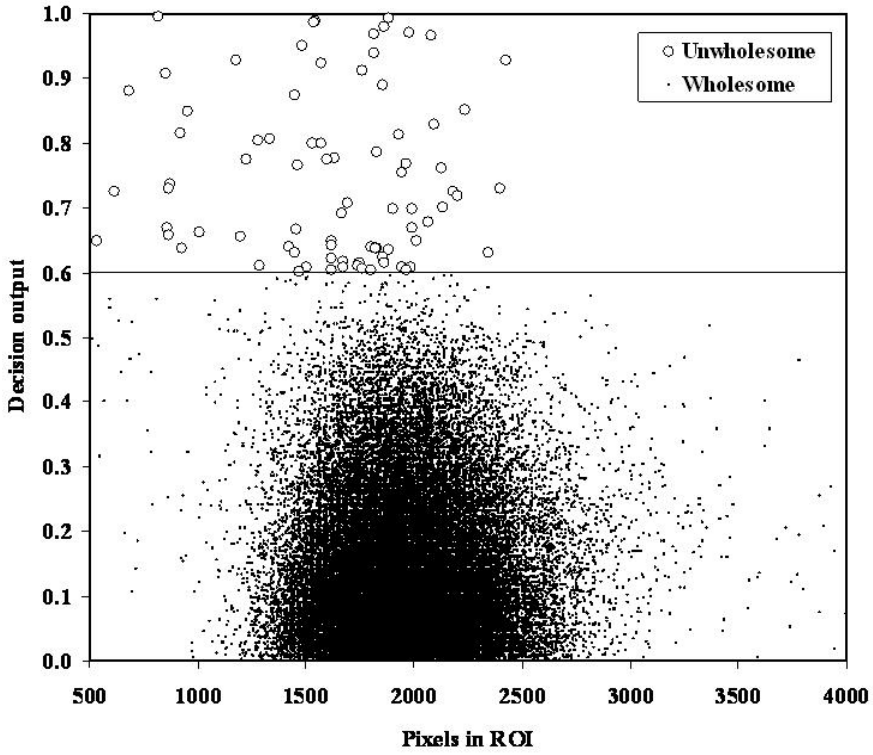

Figure 11. A scatterplot graph showing the distribution of chicken carcasses imaged during inspection shift 2, by the number of ROI pixels and the final decision output for each chicken.

Table 3. Wholesome and unwholesome birds identified during inspection shifts by processing line inspectors and by the imaging inspection system.

	Line Inspectors			Imaging Inspection System		
	Wholesome	Unwholesome	Total	Wholesome	Unwholesome	Total
Shift 1	53563 (99.84%)	84 (0.16%)	53647 (100%)	45305 (99.37%)	288 (0.63%)	45593 (100%)
Shift 2	64972 (99.89%)	71 (0.11%)	65043 (100%)	60922 (99.84%)	98 (0.16%)	61020 (100%)

A veterinarian also conducted several periods of system verification, each lasting approximately 30 to 40 min. The veterinarian conducted bird-by-bird observation of chicken carcasses immediately before they entered the IFOV of the imaging system. The imaging system output was observed for agreement with the veterinarian's identifications. The veterinarian observed 16,174 wholesome birds and 43 unwholesome birds over 4 verification periods during inspection shift 1. Of these birds, the imaging system incorrectly identified only 118 wholesome birds (99.27% correct) and 2 unwholesome birds (95.35% correct). The veterinarian observed 27,626 wholesome birds and 35 unwholesome birds over 6 verification periods during inspection shift 2. Of these birds, the imaging system incorrectly identified only 46 wholesome birds (99.83% correct) and 1 unwholesome bird (97.14% correct). These results, together with the percentages listed in table 3, strongly suggest that the imaging inspection system can perform successfully on a commercial poultry processing line.

For multispectral inspection conducted on a 140-bpm processing line was performed for this study, the imaging system acquired about 30 to 40 line-scan images between the SP and EP for each chicken inspected. Previous testing of the imaging system on a 70-bpm processing line (Chao et al., 2007) demonstrated similar performance in identification of wholesome and unwholesome birds with the analysis of about 70- to 80-line-scan images for each chicken. Because the unwholesome birds exhibit a systemic unwholesome condition affecting the entire body of the bird, this line-scan imaging system is able to identify such birds at even higher speeds; on a 200-bpm processing line, for example, the system would perform similarly in identifying wholesome and unwholesome birds by analyzing about 20- to 25-line-scan images for each chicken.

CONCLUSIONS

An online line-scan imaging system capable of both hyperspectral and multispectral visible/near-infrared reflectance was developed to inspect freshly slaughtered chickens on a processing line for wholesomeness. In-plant testing results indicated that the imaging inspection system achieved over 99% accuracy in identifying wholesome chickens and over 96% accuracy in identifying unwholesome diseased chickens. With appropriate methods of hyperspectral analysis and algorithms for online image processing, a machine vision system utilizing an EMCCD camera for multispectral inspection can satisfy both the food safety performance

standards and the high-speed production requirements (e.g., at least 140 bpm) of commercial chicken processing. Use of the imaging system may also help to improve product safety by preventing most unwholesome birds from entering the evisceration line and lowering the risk of cross-contamination. In addition, use of the system can help reduce the routine workload imposed upon FSIS inspectors working in HIMP processing plants, allowing them opportunities to perform more meaningful tasks to enhance the public health safety for poultry products.

REFERENCES

Chao, K., Y. R. Chen, H. L. Early, and B. Park. 1999. Color image classification systems for poultry viscera inspection. *Applied Engineering in Agriculture* 15(4): 363-369.

Chao, K., Y. R. Chen, W. R. Hruschka, and F. B. Gwozdz. 2002. On-line inspection of poultry carcasses by a dual-camera system. *J. of Food Engineering* 51(3): 185-192.

Daley, W., R. Carey, and C. Thompson. 1994. Real-time color grading and defect detection of food products. In *Optics in Agriculture, Forestry, and Biological Processing*, SPIE 2345: 403-411. Bellingham, Wash.: SPIE.

Delwiche, S. R. 2003. Classification of scab- and other mold-damaged wheat kernels by near-infrared reflectance spectroscopy. *Transactions of the ASAE* 46(3): 731-738.

Jing, H., X. Chen, Y. Tao. 2003. Analysis of factors influencing the mapping accuracy of x-ray and laser range images in a bone fragment inspecting system. ASAE Paper No. 033086. St. Joseph, Mich.: ASAE.

Kim, M. S., A. M., Lefcourt, and Y. R. Chen. 2003. Multispectral laser-induced fluorescence imaging system for large biological samples. *Applied Optics* 42(19): 3927-2934.

Lu, R. 2007. Nondestructive measurement of firmness and soluble solids content for apple fruit using hyperspectral scattering images. *Sensing and Instrumentation for Food Quality and Safety* 1(1): 19-27.

Park, B., and Y. R. Chen. 2000. Real-time dual-wavelength image processing for poultry safety inspection. *J. Food Proc. Engr.* 23(5): 329-351.

Tao, Y., J. Shao, K. Skeeles, and Y. R. Chen. 1998. Detection of poultry disease and enlarged spleen by computer imaging. ASAE Paper No. 983017. St. Joseph, Mich.: ASAE.

Windham, W. R., D. P. Smith, B. Park, K. C. Lawrence, and P. W. Feldner. 2003. Algorithm development with visible/near-infrared spectra for detection of poultry feces and ingesta. *Transactions of the ASAE* 46(6): 1733-1738.

USDA. 1996. Pathogen reduction: Hazard analysis and critical control point (HACCP) systems. Final rule. Fed. Reg. 61: 38805-38989.

USDA. 1997. HACCP-based inspection models project (HIMP). Proposed rule. Fed. Reg. 62:31553-31562.

USDA. 2007. Poultry production and value – 2006 summary. National Agricultural Statistics Service. Washington, D.C.